Time-domain Sparsity based Bearing Fault Diagnosis Methods Using Pulse Signal-to-noise Ratio

Chi Zhang, Shaoming Wei, Ge Dong, Yajun Zeng, Guohun Zhu, Xujuan Zhou and Feng Liu

***Abstract*—A fast and automated technique is crucial for bearing faults diagnosis during operation. To circumvent the intricacies of signal spectrum analysis, a diagnostic method named the pulse signal-to-noise ratio (PSNR) test is proposed by exploiting the time-domain sparsity of fault signals under a constant angular rate, which are modeled as periodic pulses with consistent duty cycle and power. The algorithm employs a statistic called pulse signal-to-noise ratio to both identify faults and determine their location. A simplified variant of the PSNR test, named pulse signal-to-noise amplitude ratio (PSNAR) test, is further proposed for near multiplication-free fast diagnosis. Data from Machinery Failure Prevention Technology (MFPT) and Case Western Reserve University (CWRU) were used to verify the algorithm.**

***Index Terms*—Bering fault diagnosis, generalized likelihood ratio test, low-complexity, pulse signal model, pulse signal-to-noise ratio.**

I. INTRODUCTION

BEARING failure is a frequent problem in mechanical systems. To detect and diagnose bearing faults, mechanical vibration can be monitored using accelerometers [1]. The diagnosis of bearing faults deals primarily with three types of single-point defects: outer race, inner race, and ball (roller) faults [2]. Efficiently identifying fault types remains challenging in industrial scenarios due to strong interference, and our study designs a diagnosis method that considers both accuracy and complexity.

Defects in different parts produce quasi-periodic impacts with a corresponding characteristic period (frequency) that is used to differentiate between the three fault types [3]. The most widely used approach is envelope spectrum analysis [4], which converts the signals into periodic envelope by Hilbert transform and squaring, and identifies the characteristic frequency using fast Fourier transform (FFT) [6]. Fundamentally, the analysis examines the periodic fluctuations in energy signals induced by impacts in the frequency domain [7]-[9]. Another common method is the harmonic signal-to-noise ratio (HSNR), which diagnoses the fault characteristic period via auto-correlation [10]. Despite their usefulness, these methods do not fully utilize prior knowledge, leaving room for improvement. Moreover, an automated identification of errors is desired to ensure impartial judgments [11].

On the other hand, the impulsivity of the fault pulses are well exploited to identify the most significant subband during preprocessing. Typically, the kurtogram is used to indicate the subband with maximum kurtosis [12]. Numerous similar criteria, all essentially envelope weighting, have then been presented over the past decade [13]. In recent years, studies have noticed the sparsity of bearing signals and proposed new preprocessing approaches to enhance the signal before diagnosis [14], [15]. Sparse recovery algorithms are designed to recover the fault pulses that occupy only a small portion in the time-domain with known potential characteristic period [16]. However, most sparse recovery algorithms involving optimization are computationally complex with unclear improvement in diagnostic performance [17].

This paper commences with an analysis of bearing signal, which is modelled as periodic pulses with fixed power and duty cycle, as the basis for time-domain processing. The fault diagnosis constitutes a hypothesis testing problem and a test statistic PSNR is designed for both Neyman-Pearson (NP) test-based fault detection and generalized likelihood ratio test (GLRT)-based fault classification. A low-complexity algorithm, named the PSNAR test, has been further developed by substituting the power ratio in PSNR with the amplitude ratio to achieve nearly multiplication-free fast diagnosis. Both methods exhibit satisfactory diagnostic performance with the measured data. The paper is organized as follows: Section II elaborates on the pulse signal model. Section III presents the diagnostic algorithm. Section IV verifies the method with measured data, and Section V draws a conclusion.

II. BEARING SIGNAL MODEL

Like the traditional techniques, the diagnosis is conducted by utilizing the unique pulse characteristic frequency produced by single-point defect [3]. To highlight the feature of each fault, the sampled discrete signals $\mathbf{x}=[x[0],x[1]...]$ are modeled as

$$x[k]=\begin{cases} s[k]+w[k], lT(i)+\varphi(i)\le k<lT(i)+\varphi(i)+P(i) \\ w[k], \text{ other } k \end{cases}, \quad (1)$$

where the characteristic period $T(i)$ is pre-known for specific bearings with a given shaft speed and physical structure [3]. The $i=0,1,2,$ and 3 correspond to four hypotheses: normal, outer race, inner race, and ball fault, denoted by $\mathcal{H}_0$, $\mathcal{H}_1$, $\mathcal{H}_2$, and $\mathcal{H}_3$. The pulse width is presumed to be $P(i)=\eta T(i)$, where the pulse duty cycle $\eta<1$ is the same for different $i=1, 2,$ and 3 as in [16]. $P_0=\eta=0$ for $\mathcal{H}_0$ with no fault pulse. The number

This work was supported by the National Natural Science Foundation of China under Grant No.62171029 and No.61671035. (Corresponding author: Ge Dong).

Chi Zhang and Ge Dong are with the School of Aerospace Engineering, Tsinghua University, Beijing, China.

Shaoming Wei and Yajun Zeng are with the School of Electronic and Information Engineering, Beihang University, Beijing, China.

Guohun Zhu and Feng Liu are with the School of Information Technology and Electrical Engineering, University of Queensland, St Lucia, Queensland, Australia.

Xujuan Zhou is with School of Business, University of Southern Queensland, Toowoomba, Queensland, Australia.

of pulses observed is $l=-1,0,1,2...$, where the -1 indicates that a pulse may have already occurred at the start of the observation. $0\le\varphi(i)<T(i)$ is the unknown pulse start time, and the first fully observed pulse starts at the $\varphi(i)$ th sample. $w[k]$ is white Gaussian noise with variance σ_n^2.

The $s[k]$ are modeled as random and independent samples with identical Gaussian distribution with zero mean and variance (power) σ_s^2, i.e. $s[k]\sim\mathcal{N}(0,\sigma_s^2)$. The fault pulses in all cases are considered to have identical expected energy, significantly simplifying the shape of the impact pulses and disregarding the influence of any fault location change. The sole variation among the four hypotheses is the pulse repetition time, which is used to design the following diagnostic method.

III. Method

The hypothesis $\mathcal{H}_1$, $\mathcal{H}_2$, and $\mathcal{H}_3$ can be distinguished by their different characteristic period $T(i)$. Since the probability density function of each hypothesis is unknown with unknown $\varphi(i)$, $\sigma_{s,i}^2$, and $\sigma_{n,i}^2$, the GLRT method is used to derive the diagnostic method [18]. The first step is the maximum likelihood estimation of the unknown parameters. The logarithmic likelihood function of the signal model (1) is

$$\begin{aligned}\ln\left(p\left(\mathbf{x};\varphi(i),\sigma_{s,i}^2,\sigma_{n,i}^2\right)\right)=&\\ -\frac{(1-\eta)K}{2}\ln\left(2\pi\sigma_{n,i}^2\right)-\frac{\eta K}{2}\ln\left(2\pi\left(\sigma_{n,i}^2+\sigma_{s,i}^2\right)\right)&\\ -\frac{1}{2\sigma_n^2}\sum_{l=-1}^{L(i)-1}\sum_{p=P(i)}^{T(i)-1}x^2[p+\varphi(i)+lT(i)]&\\ -\frac{1}{2\left(\sigma_{n,i}^2+\sigma_{s,i}^2\right)}\sum_{l=-1}^{L(i)-1}\sum_{p=0}^{P(i)-1}x^2[p+\varphi(i)+lT(i)],&\end{aligned}\tag{2}$$

where the p is constrained by $0\le p+\varphi(i)+lT(i)<K$ to ensure that the sample numbers are within 0 to $K-1$. The following equations all adhere to this constraint. K is the number of samples and $L(i)$ is the number of observed pulses. The K samples are assumed to contain exactly $L(i)$ pulses. Incomplete pulses may be included at the beginning and end of the observation, which are ignored because their influence is small when the number of observed pulses $L(i)$ is large. The estimated results that maximize (2) are

$$\begin{aligned}\hat\sigma_{s,i}^2+\hat\sigma_{n,i}^2&=\frac{1}{\eta K}\sum_{l=-1}^{L(i)-1}\sum_{p=0}^{P(i)-1}x^2[p+\hat\varphi(i)+lT(i)]\\&=\max\left\{\tilde{\mathbf{x}}_i\otimes[1,1...1,0...0]\right\}/\eta K,\end{aligned}\tag{3}$$

$$\hat\sigma_{n,i}^2=\frac{1}{(1-\eta)K}\left[\sum_{k=0}^{K-1}x^2[k]-\eta K\left(\hat\sigma_{s,i}^2+\hat\sigma_{n,i}^2\right)\right],\tag{4}$$

$$\hat\varphi(i)=\arg\max_{0\le\varphi(i)<T(i)}\left\{\sum_{l=-1}^{L(i)-1}\sum_{p=0}^{P(i)-1}x^2[p+\varphi(i)+lT(i)]\right\},\tag{5}$$

where the $\otimes$ means circular convolution. The constant vector $[1,\ 1...\ 1,0,...0]$ consists of $P(i)$ 1s and $T(i)-P(i)$ 0s. The vector $\tilde{\mathbf{x}}_i=\left[\tilde x_i[0],\tilde x_i[1],...,\tilde x_i[T(i)-1]\right]$ consists of $T(i)$ elements where

$$\tilde x_i[j]=\sum_{l=0}^{L(i)-1}x^2[j+lT(i)],\ j=0,1,2...,T(i)-1.\tag{6}$$

The likelihood function (2) with estimated parameters is

$$\begin{aligned}p\left(\mathbf{x};\hat\varphi(i),\hat\sigma_{s,i}^2,\hat\sigma_{n,i}^2\right)=&-\frac{(1-\eta)K}{2}\ln\left(2\pi\hat\sigma_{n,i}^2\right)\\&-\frac{\eta K}{2}\ln\left(2\pi\left(\hat\sigma_{n,i}^2+\hat\sigma_{s,i}^2\right)\right)-\frac{K}{2}.\end{aligned}\tag{7}$$

See the Appendix for proof of (3) to (7). The Eq. (7) is an increasing function of $PSNR_i=\hat\sigma_{s,i}^2/\hat\sigma_{n,i}^2\ge0$, so the likelihood ratio test is formulated as

$$\hat i=\arg\max_{i=1,2,3}\left\{p\left(\mathbf{x};\hat\varphi(i),\hat\sigma_{s,i}^2,\hat\sigma_{n,i}^2\right)\right\}=\arg\max_{i=1,2,3}\left\{\hat\sigma_{s,i}^2/\hat\sigma_{n,i}^2\right\},\tag{8}$$

where the hypothesis $\mathcal{H}_i$ that maximizes (7) is the diagnostic result in the presence of a fault.

For hypothesis $\mathcal{H}_0$, $PSNR_0=0$ and a NP test is used to determine whether the fault exists with given detection threshold γ. The bearing is considered normal if

$$\max_{i=1,2,3}\left\{PSNR_i(\mathbf{x})\right\}<\gamma,\tag{9}$$

where the γ is governed by the given false alarm rate p_f

$$p_f=p\left(\max_{i=1,2,3}\left\{PSNR_i(\mathbf{w})\right\}>\gamma\right),\tag{10}$$

where the signal $\mathbf{w}$ is white Gaussian noise with the same length and sampling rate as $\mathbf{x}$.

Both (8) and (9) use $PSNR_i$ as the test statistic, so the diagnostic method is named a PSNR test. The clear physical meaning of PSNR suggests that we can replace the signal-to noise power ratio with a simpler amplitude ratio, defined as $PSNAR_i=\hat A_{s,i}/\hat A_{n,i}$ where

$$\hat A_{s,i}+\hat A_{n,i}=\frac{1}{\eta K}\max_{\varphi(i)}\left\{\sum_{l=-1}^{L(i)-1}\sum_{p=0}^{P(i)-1}\left|x[p+\varphi(i)+lT(i)]\right|\right\},\tag{11}$$

$$\hat A_{n,i}=\sum_{k=0}^{K-1}\left|x[k]\right|-\left(\hat A_{s,i}+\hat A_{n,i}\right).\tag{12}$$

And the PSNAR test procedure follows (8) and (9), where the $PSNR_i$ is replaced by $PSNAR_i$. Both methods are shown in **Algorithm I**.

The complexity of both proposed methods is lower than that of existing methods. The PSNR test mainly involves

---

Algorithm I: Bearing fault diagnosis.

Input: Fault characteristic period $T(1)$, $T(2)$, and $T(3)$.
Pulse duty cycle η and fault detection threshold γ,
Input signal $\mathbf{x}$.

1: Calculate $\tilde{\mathbf{x}}_i$ by using $\tilde x_i[j]=\sum_{l=0}^{L(i)-1}\left|x[j+lT(i)]\right|^c$, where the exponential c is 2 for PSNR test and 1 for PSNAR test.

2: Estimate $\left(\hat A_{s,i}+\hat A_{n,i}\right)$ or $\left(\hat\sigma_{s,i}^2+\hat\sigma_{n,i}^2\right)=\max\left\{\tilde{\mathbf{x}}_i\otimes[1,...1,0...0]\right\}/\eta K$.

3: Calculate the $PSNR_i=\hat\sigma_{s,i}^2/\hat\sigma_{n,i}^2$ or $PSNAR_i=\hat A_{s,i}/\hat A_{n,i}$.

4: Compare $\max_{i=1,2,3}\left\{PSNR_i(\mathbf{x})\right\}$ or $\max_{i=1,2,3}\left\{PSNAR_i(\mathbf{x})\right\}$ with γ.

5: If γ is bigger, the bearing is considered normal. Conversely the fault type with the maximum $PSNR_i$ or $PSNAR_i$ is diagnosed.

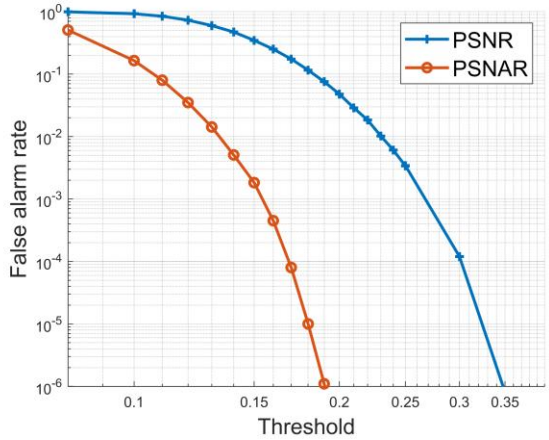

Fig. 1. False alarm rates for given detection thresholds of PSNR and PSNAR test in white Gaussian noise.

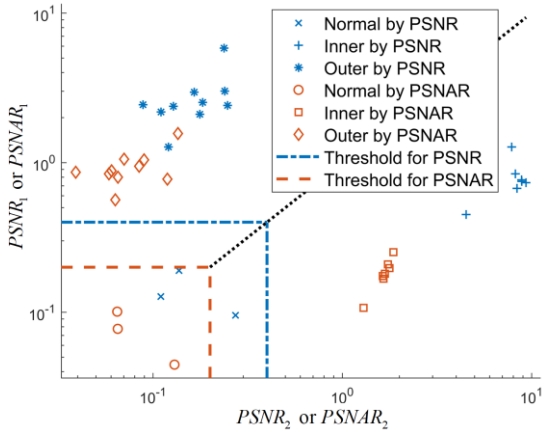

Fig. 2. PANSRs and PANSRs of data from MFPT.

multiplications in (6), where K squares are calculated. Thus, its complexity is $O(K)$, lower than spectrum or correlation based methods using FFT whose complexity is $O(K\log(K))$ [19], [20]. The PSNAR test is multiplication-free except for the only calculation of the amplitude ratio, so its complexity is significantly lower than state-of-the-art methods.

IV. Experiments and Results

A. Fault Detection Threshold

First, set the fault detection threshold for NP test. The definitions in (10) is not analytical, so 10^7 Monte Carlo simulations were conducted to determine a quantitative relationship between the detection threshold γ and false alarm rate p_f with a signal length of 0.25 seconds (3000 samples), a sampling rate of 12kHz, and a duty cycle of 0.3. Different parameters will influence simulation results, hence the following experiments also used data truncated to 0.25 seconds and assume a duty cycle of 0.3. The fault characteristic frequencies in the simulation were set as 107.3Hz, 162.4Hz, and 141.1Hz.

The results are presented in Fig. 1. When $\gamma = 0.4$ for PSNR test and $\gamma = 0.2$ for PSNAR test, the false alarm rate is less than 10^{-6}, which means that when the bearing is normal and the sensor only collects white noise, misjudgments occur once every about 10^6 diagnoses. The same threshold is used for subsequent experiments, as it is enough to detect faults with sufficient certainty and prevent frequent false alarms.

B. Diagnosis on Measured Data

The experimental data were from MFPT [21] and CWRU data center [22]. The MFPT dataset includes only outer and inner race fault data, and the diagnostic results are visualized in Fig.2, where each data is depicted as a point whose position is determined by $PSNR_1$ ($PSNAR_1$) and $PSNR_2$ ($PSNAR_2$). The plane is segregated into three decision domains, in which the data within the square region surrounded by horizontal and vertical lines satisfy (9) and are considered normal. The data above or below the diagonal line have larger $PSNR_1$ ($PSNAR_1$) or $PSNR_2$ ($PSNAR_2$), respectively. All faulty data were correctly diagnosed whilst the normal data evidently fell below the detection thresholds.

TABLE I
CWRU DATA DIFFICULT TO DIAGNOSE

	Number of successful diagnoses	Algorithm complexity
PSNR test	187(62.5%)	$O(K)$
PSNAR test	185(61.9%)	$O(K)$
Envelope Spectrum	181(60.5%)	$O\left(K\log(K)\right)$
HSNR	167(55.9%)	$O\left(K\log(K)\right)$
CMS	179(59.9%)	$O\left(N_w N_{STFT}\log(N_{STFT})+N_{STFT}N_w\log(N_w)\right)$
Fast-SC	186(62.2%)	$O\left(N_w N_{STFT}\log(N_{STFT})+N_P N_{STFT}N_w\log(N_w)\right)$
Number of data	299(100%)	

The CWRU data poses greater diagnostic difficulty with many anomalous data [4]. 299 sets of drive-end and fan-end bearing fault data sampled at 12kHz were utilized in experiment. The Envelope analysis [4], cyclic modulation spectrum (CMS) [8], fast spectral correlation (Fast-SC) [9], and HSNR [10] were used for comparison. Given the lack of unified fault detection criteria, it is assumed that a known fault is present and only determine the fault type by seeking the most significant fault features. For the proposed method, the detection threshold is 0, and the hypothesis with the largest $PSNR_i$ or $PSNAR_i$ is taken as the result.

Table I presents the diagnostic accuracy of six methods. The PSNR test and the simplified PSNAR test produced almost identical results. The two proposed methods yielded slight advantages over the classical envelope spectrum and were akin to the enhanced envelope spectrum obtained by fast-SC. Numerous anomalous data in CWRU dataset created great challenges for all methods, and the both proposed methods demonstrated no inferior performance compared to other contemporary methods.

Besides, the proposed method has great complexity advantages. In Table I, the N_w and N_{STFT} are the windows number and FFT length in short time Fourier transform of input signal. The N_P is

the number of frequency bins used for correlation in Fast-SC [9]. Due to the overlaps in short-time Fourier transform, the product of N_w and N_{STFT} is much larger than the signal length K, leading to an high complexity of CMS and Fast-SC.

V. Conclusion

An automated bearing fault diagnosis method named PSNR test is designed, which employs the PSNR as the criterion for fault detection and classification. A simplified PSNAR test is further developed by substituting signal squares in PSNR test with absolute values. Both methods have low complexity, especially the latter. The proposed time-domain signal model is primitive and future research with more accurate model would further optimize the algorithm.

Appendix

First, estimate the sum of signal and noise power $\left(\sigma_{n,i}^2+\sigma_{s,i}^2\right)$ by making (2) derivative to $\sigma_{s,i}^2$ 0

$$-\frac{\eta K}{2\left(\sigma_{n,i}^2+\sigma_{s,i}^2\right)}+\frac{\sum_{l=-1}^{L(i)-1}\sum_{p=0}^{P(i)-1}x^2[p+\varphi(i)+lT(i)]}{2\left(\sigma_{n,i}^2+\sigma_{s,i}^2\right)^2}=0, \quad (13)$$

whose solution is

$$\sigma_{s,i}^2+\sigma_{n,i}^2=\frac{1}{\eta K}\sum_{l=-1}^{L(i)-1}\sum_{p=0}^{P(i)-1}x^2[p+\varphi(i)+lT(i)]. \quad (14)$$

Similarly, make the (2) derivative to $\sigma_{n,i}^2$ 0 and

$$\sigma_{n,i}^2=\frac{1}{(1-\eta)K}\sum_{l=-1}^{L(i)-1}\sum_{p=P(i)}^{T(i)-1}x^2[p+\varphi(i)+lT(i)]. \quad (15)$$

Estimate $\varphi(i)$ by maximizing the likelihood function in (2), with (14) and (15) substituted

$$\hat{\varphi}_i=\arg\max_{0\le\varphi(i)<T(i)}\left\{-\frac{K}{2}\left[\begin{matrix}(1-\eta)\ln\left(2\pi\sigma_{n,i}^2\right)+\\ \eta\ln\left(2\pi\left(\sigma_{s,i}^2+\sigma_{n,i}^2\right)\right)+1\end{matrix}\right]\right\}, \quad (16)$$

which includes the summation of K convex ln() functions, whose variables satisfy that

$$(1-\eta)K\sigma_{n,i}^2+\eta K\left(\sigma_{s,i}^2+\sigma_{n,i}^2\right)=\sum_{k=0}^{K-1}x^2[k], \quad (17)$$

which holds for any φ_i with $i=1,2,3$. The likelihood function in (2) and (16) can be rewritten with unique variable $\sigma_{s,i}^2/\sigma_{n,i}^2$

$$\begin{aligned}\ln\left(p(\mathbf{x};\varphi_i,\sigma_{s,i}^2,\sigma_{n,i}^2)\right)&=\frac{K}{2}\ln\left(2\pi\left(\eta\sigma_{s,i}^2/\sigma_{n,i}^2+1\right)\right)-\\ &\frac{\eta K}{2}\ln\left(2\pi\left(\sigma_{s,i}^2/\sigma_{n,i}^2+1\right)\right)-\frac{K}{2}\ln\left(\frac{1}{K}\sum_{k=0}^{K-1}x^2[k]\right)-\frac{K}{2}\end{aligned} \quad (18)$$

which is increasing when $\sigma_{s,i}^2/\sigma_{n,i}^2>0$. And $\sigma_{s,i}^2/\sigma_{n,i}^2$ is an increasing function of $\sigma_{s,i}^2$, so (16) becomes

$$\hat{\varphi}(i)=\arg\max_{0\le\varphi(i)<T(i)}\left\{\sigma_{s,i}^2\right\}, \quad (19)$$

which is (5). Eqs. (3) and (4) are obtained by substituting $\hat{\varphi}(i)$ into (14) and (15). The likelihood function in (7) is similar to (18), where $\sigma_{s,i}^2/\sigma_{n,i}^2$ is replaced by $PSNR_i$.

References

[1] J. Wang, Y. Peng, and W. Qiao, "Current-aided order tracking of vibration signals for bearing fault diagnosis of direct-drive wind turbines," *IEEE Trans. Ind. Electron.*, vol. 63, no. 10, pp. 6336–6346, Oct. 2016.

[2] D. Wang, K. Tsui and Q. Miao, "Prognostics and Health Management: A Review of Vibration Based Bearing and Gear Health Indicators," *IEEE Access*, vol. 6, pp. 665–676, 2018.

[3] R. B. Randall and J. Antoni, "Rolling element bearing diagnostics—A tutorial," *Mech. Syst. Signal Process.*, vol. 25, pp. 485–520, Feb. 2011.

[4] W. Smith and R. B. Randall, "Rolling element bearing diagnostics using the Case Western Reserve University data: A benchmark study," *Mech. Syst. Signal Process.*, vol. 64–65, pp. 100–131, Apr. 2015.

[5] Y. Cheng, Z. Wang and W. Zhang, "Combined Square Envelope Spectrum by Integrating Multiband Bearing Fault Information," *IEEE Sens. J.*, vol. 23, no. 3, pp. 2495-2506, 1 Feb.1, 2023.

[6] M. Riera-Guasp, J. A. Antonino-Daviu and G. -A. Capolino, "Advances in Electrical Machine, Power Electronic, and Drive Condition Monitoring and Fault Detection: State of the Art," *IEEE Trans. Ind. Electron.*, vol. 62, no. 3, pp. 1746–1759, Mar. 2015.

[7] M. Tang, Y. Liao, R. Duan, J. Xue and X. Zhang, "Bearing Fault Diagnosis Based on the Maximum Squared-Enveloped Multipoint Kurtosis Morphological Deconvolution," *IEEE Trans. Instrum. Meas.*, vol. 71, pp. 1–11, 2022.

[8] J. Antoni and D. Hanson, "Detection of Surface Ships From Interception of Cyclostationary Signature With the Cyclic Modulation Coherence," *IEEE J. Ocean. Eng.*, vol. 37, no. 3, pp. 478-493, July 2012.

[9] J. Antoni, G. Xin, N. Hamzaoui, "Fast computation of the spectral correlation," *Mech. Syst. Signal Process*., vol. 92, pp. 248–277, 2018.

[10] X. Xu, M. Zhao, J. Lin, and Y. Lei, "Envelope harmonic-to-noise ratio for periodic impulses detection and its application to bearing diagnosis," *Measurement*, vol. 91, pp. 385–397, Sep. 2016.

[11] P. Bhonde, A. Panchwadkar, "Automatic detection of bearing faults," *Materials Today: Proceedings*, vol. 77, pp. 586–591, Nov. 2022.

[12] J. Antoni, "Fast computation of the kurtogram for the detection of transient faults," *Mech. Syst. Signal Process.*, vol. 21, no. 1, pp. 108–124, Jan. 2007.

[13] D. Wang, Z. Peng, L. Xi, "The sum of weighted normalized square envelope: A unified framework for kurtosis, negative entropy, Gini index and smoothness index for machine health monitoring," *Mech. Syst. Signal Process.*, vol. 140, Jun. 2020.

[14] Q. Zhou, Y. Zhang, C. Yi, J. Lin, L. He, and Q. Hu, "Convolutional sparse coding using pathfinder algorithm-optimized orthogonal matching pursuit with asymmetric Gaussian chirplet model in bearing fault detection," *IEEE Sens J.*, vol. 21, no. 16, pp. 18132–18145, Aug. 2021.

[15] Y. Qin, "A new family of model-based impulsive wavelets and their sparse representation for rolling bearing fault diagnosis," *IEEE Trans. Ind. Electron*., vol. 65, no. 3, pp. 2716–2726, Mar. 2018.

[16] Z. Zhao, S. Wu, B. Qiao, S. Wang and X. Chen, "Enhanced Sparse Period-Group Lasso for Bearing Fault Diagnosis," *IEEE Trans. Ind. Electron.*, vol. 66, no. 3, pp. 2143–2153, Mar. 2019.

[17] W. He, Y. Ding, Y. Zi , I. W. Selesnick, "Sparsity-based algorithm for detecting faults in rotating machines," *Mech. Syst. Signal Process.*, vol. 72–73, pp. 46–64, May. 2016.

[18] E. Fisher, J. Tabrikian and S. Dubnov, "Generalized Likelihood Ratio Test for Voiced-Unvoiced Decision in Noisy Speech Using the Harmonic Model," *IEEE Trans. Audio Speech Lang. Process*., vol. 14, no. 2, pp. 502–510, Mar. 2006.

[19] W. Wu, C. Yi, J. Bai, Y. Huang and J. Lin, "Envelope Harmonic Noise Ratio Based Adaptive Kurtogram and Its Application in Bearing Compound Fault Identification," *IEEE Sens. J.*, vol. 22, no. 9, pp. 8701-8714, May. 2022.

[20] L. Hua, X. Wu, T. Liu and S. Li, "The Methodology of Modified Frequency Band Envelope Kurtosis for Bearing Fault Diagnosis," in *IEEE Trans. Ind. Inform*., vol. 19, no. 3, pp. 2856-2865, Mar. 2023.

[21] E. Bechhoefer, "Condition Based Maintenance Fault Database for Testing Diagnostics and Prognostic Algorithms," 2013. [Online]. Available: https://mfpt.org/fault-data-sets/.

[22] Case Western Reserve University Bearing Data Center. [Online]. Available: https://engineering.case.edu/bearingdatacenter.